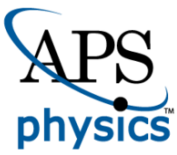

Structure, biomimetics, and fluid dynamics of fish skin surfaces*

George V. Lauder, Dylan K. Wainwright, August G. Domel, James C. Weaver, Li Wen, and Katia Bertoldi

Phys. Rev. Fluids **1**, 060502 — Published 18 October 2016

DOI: 10.1103/PhysRevFluids.1.060502

Structure, biomimetics, and fluid dynamics of fish skin surfaces

George V. Lauder[1*], Dylan K. Wainwright[1], August G. Domel[2], James C. Weaver[3], Li Wen[4], and Katia Bertoldi[2]

[1*] *Museum of Comparative Zoology, and Department of Organismic and Evolutionary Biology, Harvard University, Cambridge, MA 02138*

[2] *School of Engineering and Applied Sciences, Harvard University, Cambridge, MA 02138*

[3] *Wyss Institute for Biologically Inspired Engineering, Harvard University, Cambridge, MA 02138, USA*

[4] *School of Mechanical Engineering and Automation, Beihang University, Beijing, 100191, People's Republic of China*

(Dated August 23, 2016)

* Author for correspondence (George V. Lauder: glauder@oeb.harvard.edu)

ABSTRACT

The interface between the fluid environment and the surface of the body in swimming fishes is critical for both physiological and hydrodynamic function. The skin surface in most species of fishes is covered with bony scales or tooth-like denticles (in sharks). Despite the apparent importance of fish surfaces for understanding aquatic locomotion and near-surface boundary layer flows, relatively little attention has been paid to either the nature of surface textures in fishes or possible hydrodynamic effects of variation in roughness around the body surface within an individual and among species. Fish surfaces are remarkably diverse and in many bony fishes scales can have an intricate surface texture with projections, ridges, and comb-like extensions. Shark denticles (or scales) are tooth-like, and project out of the skin to form a complexly textured surface that interacts with free-stream flow. Manufacturing biomimetic foils with fish-like surfaces allows hydrodynamic testing, and we emphasize here the importance of dynamic test conditions where the effect of surface textures is assessed under conditions of self-propulsion. We show that simple two-dimensional foils with patterned cuts do not perform as well as a smooth control surface, but that biomimetic shark skin foils can swim at higher self-propelled speeds than smooth controls. When the arrangement of denticles on the foil surface is altered, we find that a staggered-overlapped pattern outperforms other arrangements. Flexible foils made of real shark skin outperform sanded controls when foils are moved with a biologically realistic motion program. We suggest that focus on the mechanisms of drag reduction by fish surfaces has been too limiting, and an additional role of fish surface textures may be to alter leading edge vortices and flow patterns on moving surfaces in a way that enhances thrust. Analysis of water flow over an artificial shark skin foil under both static and dynamic conditions shows that a shear layer develops over the denticle surface, and we propose that there is limited flow under the expanded surfaces of shark denticles. The diversity of fish scale types and textures and the effect of these surfaces on boundary layer flows and fish locomotor energetics is a rich area for future investigation.

I. INTRODUCTION

For a swimming fish, the interface between the fluid environment and the body is critical for both physiological and hydrodynamic function. Processes such as the exchange of ions, carbon dioxide, and oxygen all occur across the surface area of body tissues, and frictional and pressure forces that arise during locomotion are significantly affected by surface texture and conformation. Interfacial phenomena are of general importance in biofluid dynamics, but for swimming fish, the nature of the interface between the body and fluid is a key factor determining both the energetic cost of locomotion in the short term, as well as being responsible for evolutionary specializations such as drag reducing features on longer time scales.

Despite the apparent importance of fish surfaces for understanding aquatic locomotion, relatively little attention has been paid to the nature of the skin surface texture in fishes and the possible hydrodynamic effects of variation in texture around the body surface as well as among species. For example, the surfaces of bony fish are substantially different from the skin surface of sharks and rays, and yet we understand little about the hydrodynamic consequences of these different surface types. Furthermore, the three-dimensionality of biological fish surfaces is not well characterized, and the extent to which textural elements extend into the boundary layer as fish swim is unknown, as is the extent of movement (either active or passive) among skin surface elements. Moreover, there are few experimental models that can replicate *in vivo* fish surface function during locomotion and allow measurement of parameters such as swimming speed, the energetic cost of locomotion, and thrust and drag forces under dynamic swimming conditions.

Fish surfaces are composed of arrays of individual scales (often termed denticles in sharks and rays) that form a textured surface. In sharks, the denticles have a complex shape (see below) and penetrate the epidermal skin layer to make direct contact with the water. Shark denticles are homologous to mammalian teeth [1]: each denticle possesses an interior pulp cavity with nervous and arterial supply, a coating of dentine and enamel, as well as a "root" or expanded base embedded within the dermis. In bony fish, individual scales are composed of bone arranged in thin layers to make a laminated composite structure [2-4]. Scales are embedded within the skin's epidermal layer, and in most species scales do not make direct contact with the water due to the epidermal coating. Bony fish surfaces are also often well-supplied with mucus glands, and a mucus coating can obscure some features of scale surface texture.

The skin of sharks has attracted the most attention as a biological surface that might possess special drag-reducing properties in the water, and a number of simple physical models have been suggested that might replicate shark-skin function [5-10]. These studies have focused on static testing, analyzing drag forces on rigid surfaces as a function of flow speed, and examining the effect of surface feature spacing on the magnitude of observed drag reduction. Riblet models as a general abstraction of a shark-like textured surface also have been analyzed for drag reducing properties [8,11-13], and recent computational models have assessed the ability of shark skin surfaces to possibly reduce drag [14,15], again under static conditions.

In considering the effect of surface structures on drag, it is useful to consider both the Reynolds number and a dimensionless S+ number [5,16,17]. However, the characteristic length scale for Reynolds numbers relevant to fish locomotion can range from propulsor (or fish) body length, down to the spacing between surface roughness elements and boundary layer thickness. For the types of data and experiments described here, whole propulsor (foil or animal) Re ranges from ~$1 * 10^3$ to $2 * 10^5$ although large pelagic fishes such as tuna certainly swim at higher Re than this. Using the distance between adjacent riblet-like ridges on shark skin denticles as a characteristic length, and free-stream flow velocities of typical laboratory experiments in water, the Re is on the order of 15. Clearly a range of interesting fluid dynamic phenomena may be involved in understanding how fish scales interact with their fluid environment.

In addition, the dimensionless S+ parameter has been used in studies of drag reduction as the Reynolds number may not be the most relevant metric when fish surface structures have a much smaller size scale than that of the whole body [13,17-19]. S+ is a function of the spacing between surface projections, fluid kinematic viscosity, density, and average surface shear stress. Values of S+ between approximately 5 and 25 have been shown to represent conditions where surface textures may result in reduced friction drag.

In this paper we present an overview of fish surface structures and their hydrodynamic effects studied under dynamic conditions. First, we provide a synopsis of the diversity of three-dimensional fish surfaces. There is a remarkable and unappreciated diversity of fish surface textures, and new technologies have recently allowed measurement of the surface topography of fish skin. Second, we discuss experimental platforms that allow dynamic testing of a variety of alternative fish surface designs that range from simple two-dimensional physical models to 3D-printed shark skin, to pieces of actual shark skin. Finally, we present the results of dynamic tests

of swimming performance of these different skin models, and review previous hydrodynamic results suggesting that fish skin textures may enhance propulsion by improving thrust, in addition to possible effects of drag reduction.

We believe that the near-exclusive focus on the possibility of drag reduction by fish surfaces has been too limiting, and that an additional role of fish surface textures may be to alter leading edge vortices and flow patterns on moving surfaces in a way that enhances thrust. Most importantly, we wish to emphasize the importance of dynamic testing in which model fish skin surfaces are analyzed under time-dependent conditions. Replicating the locomotor conditions of freely-swimming fishes to test hydrodynamic effects of surface structures is critical; bending of the body and active motion of fins are key features of fish propulsion [20-22]. We believe that static testing circumstances, which do not replicate patterns of skin bending, changing angles of attack through time, and self-propulsion where thrust and drag forces are balanced over a flapping cycle, are unlikely to reveal the key physical phenomena associated with fish skin surface effects during aquatic propulsion.

II. MATERIALS AND METHODS

A. Imaging

Imaging fish surfaces is challenging. In particular, imaging the surface of live fishes and the broader pattern of surface elements so that the arrangement of textural elements can be seen as they occur *in vivo* poses special difficulties. Traditionally, scanning electron microscopy (SEM) has been used to image bony fish scales, but published SEM images are almost exclusively of individual scales and do not reveal the overlapping patterns of scales and associated soft tissues in bony fishes. SEM has also been used to image the surfaces of shark skin [Figure 1; 23,24], and micro-computed tomography (μCT) scans have provided surface images of shark skin scales (or denticles) as well as for one species of bony fish [25]. For the smaller surface features of shark skin scales to be seen, μCT scanning at a resolution on the order of a micron may be necessary [19], and such scans have been used to make three-dimensional models of the individual denticles for additive manufacturing of biomimetic shark skin [26].

A new approach to imaging the surface of fish skin that provides images relevant to both propulsion and measurement of surface textural roughness is to use gel-based contact surface profilometry [27,28]. Wainwright and Lauder [25] used contact profilometry to analyze the

textures of scale patterns on the surface of bluegill sunfish, and below we provide sample images using this technique for several species of both bony fishes and sharks (Figures 2, 3).

B. Foil manufacture

In order to study the hydrodynamic effect of fish surface textures under dynamic conditions of self-propulsion where fish skin or skin models are moved with a heave (side to side) or pitch (rotational) motion program to generate thrust, fish skin models must be assembled into flexible foils or panels that can be attached to mechanical controllers. To generate simple two-dimensional physical models with patterned surfaces in which water can flow from one side of the swimming panel to the other, we used a laser cutter to slice differently shaped "scales" into flexible plastic panels (Artus color-coded shim stock; http://www.artuscorp.com) that vary in stiffness (Figure 4). Cutting shapes into plastic panels of various stiffnesses allowed individual elements to "pop-up" from the panel surface during swimming. The propulsive performance of these different patterns was tested as described below under several movement programs.

To produce membranes of shark skin for hydrodynamic testing, Oeffner and Lauder [29] excised pieces of skin from freshly caught sharks (Figure 8A), cleaned the skin samples of underlying muscle and connective tissue to produce strips of skin (Figure 8B), and assembled these strips into both rigid (by gluing skin strips to aluminum panels) and flexible (by gluing the skin strips to each other and attaching them to a leading edge rod, Figure 8C) panels for testing. The swimming performance of these skin strip panels was compared to panels in which the surface denticles had been carefully sanded off [29].

To manufacture biomimetic shark skin that allowed us to control both denticle structure and arrangement on the panel surface, we used micro-CT (μCT) scanning to generate a three-dimensional denticle model, arranged the individual model denticles into arrays of various types, and used additive manufacturing to print artificial shark skin membranes in which the denticles are made of rigid material with their expanded bases embedded into a flexible substrate (Figure 5). This approach allowed us to generate flexible biomimetic skin models in which denticles change their relative spacing as the skin changes from concave to convex during undulatory propulsion (Figure 5F). Both denticle-covered artificial shark skin membranes and the smooth controls have near identical flexural stiffnesses, due to the central supporting plastic element (Fig. 9C) to which the flexible foil surfaces were attached. This central plastic support

dominates the flexural stiffness of the entire assembly, and the presence of denticles did not noticeably alter flexural stiffness.

To explore the possibility of printing shark-like denticles at very small size scales, we used a Nanoscribe printer (Photonic professional, GmbH, Germany) and two-photon lithography to fabricate a single shark skin denticle at a size that is ten times smaller than its real scale. Figure 6 shows the optical and SEM images of a 3D-printed single shark skin denticle attached to a glass coverslip. The shark skin denticle model was first designed in Solidworks (Solidworks Corp., Waltham, MA, USA), and then converted into volumetric pixels in Matlab. UV-curable photoresist material (IP-Dip, Nanoscribe, GmbH, Germany) was exposed by a laser beam at the positions of the volumetric pixels following the designed denticle shape. A thin layer of post-exposed baked SU-8 resist material was used to ensure the polymerized shark skin denticle reliably bonded to the underlying glass coverslip for SEM imaging. Polymerizing the single shark skin denticle (15μm in length and 10μm in width) took approximately 25 minutes. Once the polymerization process was finished, unexposed regions including the denticle undercut area were removed with a developer bath using 2-methoxy-1-methylethyl acetate (PGMA). After baking the polymerized denticle at 120 °C for 30 min, the solidified shark skin denticle is rigid with a Young's modulus of approximately 4Gpa.

C. Hydrodynamic testing

Dynamic testing of fish skin model panels and membranes made from real shark skin was accomplished with a mechanical controller that allows programming of heave (side-to-side) and pitch (rotational) motions [30]. Foils are held at the leading edge by a supporting rod, which is in turn attached above the water to heave and pitch motors through a force/torque sensor (see Figures 8C and 9A). A recirculating water flow tank with programmable speed control allows testing of diverse swimming motions under a range of speeds. A number of recent studies of the dynamics of swimming flexible panels have used this apparatus to measure swimming forces and torques with a 6-axis ATI nano-17 transducer (ATI Inc., Apex, NC) [e.g., 31,32-35]. Synchronized high-speed video cameras allow measurement of foil motion as forces are recorded.

Measurement of the self-propelled swimming speed of foils is accomplished by first picking a particular motion program of heave, frequency, and pitch, and then measuring the mean thrust

across a range of imposed flow speeds. Self-propulsion, for a particular motion program, occurs at the speed where the average thrust over a flapping cycle is zero.

Flow visualization over the surface and in the wake of flapping foils is accomplished using particle image velocimetry as in our previous research. We have analyzed the vortical structure on the surface of swimming foils [19,29], and in the wake [e.g., 36,37,38] to document how changing surface characteristics and motion patterns alter flow structures. Here we present flow visualizations over the surface of a static and dynamic biomimetic shark skin foil with widely spaced denticles (arrangement of Figure 5I) to allow flow in between individual denticles to be seen, as well as the pattern of surface flow (Figure 10).

III. RESULTS

A. Fish surface topography

There is considerable regional variation in fish scale structure, and different locations on the body can have scales with dramatically different morphology [25]. In sharks (Figure 1), scales near the leading edge of the head tend to be more paver-like with flattened and smooth upper surfaces exposed to the water, while along the body the scale surface has ridges and three or more posterior finger-like projections [23,29]. Images and elevation profiles of blue shark (*Prionace glauca*) denticles (Figure 2) also show the smooth upper surface of each denticle at the front (leading edge) of the head, and ridged surfaces on denticles further back along the body. The amplitude of surface roughness in blue sharks ranges from 40 μm near the head to almost 80 μm along the body (Figure 2), and denticles are not covered by epidermis so this texture would be seen by water moving over the undulating body and tail. There is a great diversity of sizes and shapes of shark denticles [see, e.g., 39]. Sizes of individual denticles range from approximately 120 μm in open ocean sharks to more than 1 mm [39] in more benthic and slow-moving species, and denticles may be widely spaced or can be arranged in close proximity with essentially no gaps among denticles (Figure 2). Denticles of moderate to fast-swimming species have overlapping posterior extensions so that an individual upstream denticle overlaps the surface of the next downstream denticle (Figure 5A). Denticles in shark species with this overlapping structure are generally arrayed into a staggered pattern (Figure 2) where adjacent rows are offset from each other (also shown schematically in Figure 5G).

In bony fish (Figure 3), there is also variation around the body in scale structure [25]. Bony fish scales overlap considerably and approximately half of each individual scale overlaps the next most anterior scale (Figure 3B). Scales are flattened and are arranged into a tight array; surface profiles again show approximately a 40 – 50 μm surface topography, although some of the smaller-scale roughness would be covered by epidermis in life. A survey of bony fish scale topography using gel-based surface contact profilometry reveals a great diversity of surface structures that vary considerably in amplitude. Four examples of this diversity are shown in Figure 3. The exposed portion of scales can have numerous posteriorly-pointing ridges, be covered with prominent bumps, have smooth posterior edges, or possess large central ridges surrounded by smaller surface projections.

B. Swimming dynamics of biomimetic fish surfaces

Although we initially believed that the use of simple flexible (essentially two-dimensional) panels with patterned cuts that could bend and flex and "pop-up" away from the panel surface during locomotion and allow water to pass from one side to the other (Figure 4) would enhance propulsion, we were unable to find any foil of this type that outperformed a smooth control. For example, Figure 7 shows the results of measuring the self-propelled swimming speed of two different cut foils. The high-aspect ratio cut (Figure 4D) swam dramatically slower, at approximately one-fourth the speed of the smooth control (Figure 7A), and the cut foil exhibited an increased mean cost of transport (in Joules/m) nearly five times that of the control.

The cut foil pattern shown in Figure 4A was tested under two different motion programs, one with heave and pitch continually adjusted to give a zero angle of attack [see 40] (Figure 7B), and one with heave-only motion at the leading edge (Figure 7C). In both cases, the cut foil swam more slowly, and exhibited an increase in the cost of transport. While we did not explore a large parameter space of possible motion programs, and the possibility remains that some other movement patterns of these cut panels could result in improved swimming performance, we believe that the reduced effective surface area as the cut elements bend away from the panel surface reduces swimming performance in most cases. Fluid flow from one side of the panel to the other may indeed change swimming dynamics, but quantifying this effect remains a future task.

Swimming tests of *flexible* panels made from actual shark skin (Figure 8) demonstrated that for a variety of motion programs, both with pitch and heave-only, the intact shark skin surface resulted in improved self-propelled speeds compared to a control in which the surface denticles were removed by sanding. Oeffner and Lauder [29] noted, however, that their tests of *rigid* shark skin panels attached to aluminum plates (which are not able to bend) did *not* show improved swimming performance: intact skin either performed similarly to sanded skin, or in one case worse than the control. These data provide evidence that *flexibility* of the skin membranes is critical to generating improved propulsive performance.

Analysis of the swimming speeds of biomimetic shark skin panels relative to a 3D-printed control of the same mass (Figure 9C), tested at a heave amplitude and frequency of ±1.5 cm and 1Hz respectively, but at a variety of pitch values, shows that the shark skin surface swims significantly faster than the control at the intermediate pitch values of 5 to 15°, but slower or equivalently at lower and higher pitch angles. The effect of a shark skin-like surface thus depends on the movement pattern, and we should not expect improved performance under all motion programs.

Modifying the pattern of biomimetic shark skin denticles on the foil surface (Figure 9D) significantly affects propulsion, and under the test conditions of 1 Hz flapping frequency with no pitch, the staggered array of denticles (Figure 5G) performs much better than a linear array and also better than the smooth control, without any increase in the cost of transport at the lower heave motions [26].

Analysis of the pattern of water flow over the surface of shark skin compared to a sanded control showed that the roughened surface alters the intensity and location of the leading vortex formed during the flapping motion [29]. Oeffner and Lauder [29] suggested that due to the timing of flow separation and the location of the vortex center closer to the foil surface, denticles on shark skin may enhance thrust by increasing leading edge suction. Shark tails appear to possess an attached leading edge vortex during most phases of the tail beat [41], and the textured surface thus can act as a thrust-enhancer in body regions where flow separates at appropriate times in the undulatory cycle. Flow separation has also been observed on shark pectoral fins during maneuvering when pectoral fins change their angle of attack, but does not occur during steady swimming, at least when smaller sharks swim freely under laboratory conditions [42,43]. In addition, the cost of transport in flexible biomimetic shark membranes with overlapping

denticles is increased under certain motion programs, which suggests that physical interactions among denticles are increasing the flexural stiffness of the membrane during swimming, and therefore could be reduced by making each denticle slightly mobile at the base [26]. In fact, mobile denticle bases have been noted in mako sharks [23,44], and this mobility may function to reduce the cost of bending the skin back and forth, where contact among adjacent scales would otherwise increase skin bending stiffness. However, many other sharks such as leopard sharks and spiny dogfish do not possess highly flexible denticles, and the extent to which different shark species possess mobile denticles is currently unknown. For bony fish, relative motion of scales is most likely common, although scale movement during locomotion has never been measured, and the forces needed to bend bony fish skin are unknown.

One key question that remains unanswered is the extent to which water penetrates the layer of denticles on shark skin and forms vortices underneath the expanded and ridged outer surfaces. Such vortex formation might increase drag [14], but to date there are no experimental observations of such flows. Given the extensive surface provided by the upper regions of denticles (Figure 2), it might seem unlikely that there is significant flow among the denticle stalks that protrude from the epidermal surface. Studying a model system with widely spaced denticles in which such flows are visible could provide an indication of the extent of within-denticle flow, because observing such flows in freely-swimming sharks represents substantial challenges that are not likely to be resolved any time soon. Figure 10 shows the results of both static and dynamic (flapping) flow visualization using the biomimetic denticle membrane of Figure 5I. The relatively wide spacing of the denticles allows visualization of the flow in between adjacent denticles, as well as analysis of near-denticle surface flows. Although some flow can be seen separating behind denticles and forming a recirculation zone for both static and dynamic cases, a well-developed shear layer forms over the top of the denticles and across the gaps between adjacent denticles (Figure 10 C, F). This suggests that water may interact with the ridged denticle surface but not form internal vortical patterns that affect propulsion as has been previously suggested for widely spaced and erect denticles [45]. And the observation of such a distinct surface shear layer in a model system with widely-spaced denticles strongly suggests that in tightly-packed natural denticle configurations as shown in Figure 2, that sub-surface among-denticle flows could be minimal, especially if a mucus coating exists above the epidermis and around the denticle stalks.

IV. DISCUSSION

Perhaps the most significant issue for which we still lack a clear answer is the extent to which the surface structures on fish skin discussed here interact with near-surface flows and affect the boundary layer. Measurements of vortex location on the surface of swimming panels of shark skin allowed measurement of flow within a few millimeters of the skin surface, and were able to detect alterations in vortex structure when denticles were removed [29]. But boundary layer profiles have yet to be measured on panels of flapping shark skin. Some fish skin structures can project hundreds of microns above the mean surface, and it is likely that surface roughness has significant effects on flow near the surface and alters the boundary layer profile compared to a smooth surface. In order to understand the functional significance of the diversity of fish surface structures, we need to measure boundary layer profiles along the body during swimming, as static models will not reflect the effects of pressure gradients that develop as the body bends back and forth, and pressure changes substantially along the fish body during locomotion [46].

Quantifying boundary layer profiles along the length of swimming fishes is challenging, and high resolution and high frequency imaging of flows in small areas on the order of 1-5 mm^2 are needed to visualize boundary layer profiles and their evolution through time. The boundary layer of freely-swimming fishes has only been measured in two previous studies, and in both cases it was not possible to determine the effect of surface roughness on flow structure or separation point. The first paper to measure the boundary layer of a swimming fish is that of Anderson et al. [47] who were able to quantify profiles along the body in one bony fish species (scup, *Stenotomus chrysops*), and one shark, the smooth dogfish (*Mustelus canis*) during free swimming. They showed that there was little flow separation along the body at the swimming speeds studied (Reynolds numbers up to 3×10^5) and proposed that there is minimal body pressure drag at these speeds. Furthermore, their results suggest that there is substantially increased total friction on an undulating fish body compared to the same rigid body towed at the swimming speed. A similar conclusion that body undulations increase frictional drag forces has been reached by [48,49], who support the "Bone-Lighthill hypothesis" that changes in boundary layer thickness as a result of body undulation increase frictional drag forces.

Yanase and Saarenrinne [50] have recently measured boundary layer profiles on the body surface of trout swimming at a Reynolds number of 4×10^5, and have shown that boundary layers can be unsteady and turbulent at certain locations on the fish. These authors report finding small recirculation regions near the trout surface that are similar to laminar separation bubbles that result from adverse pressure gradients and cause flow separation. Areas of flow separation result in *upstream* flow at the skin surface at this localized region. Because trout possess small scales that are coated with a mucus layer, and the trout skin surface is thus very smooth, we do not expect to see effects of scales on boundary layer profiles in this species. But in other bony fish such as bluegill sunfish where the scales on many regions of the body have posteriorly projecting small "teeth" or ctenii [25] that pierce the mucus layer and enter the boundary layer, such effects may be evident (Figure 3).

We emphasize the importance of measuring the local flow environment on the skin surface to understand the effect of different scale structures on boundary layer flow. If there are regions of flow separation, then flow at the skin surface will be moving in the *opposite* direction to the free stream, and scales with ctenii or other asymmetrical shapes and features may function very differently than if flow were uniformly downstream along the body. Such an effect has been seen in swimming shark skin membranes [29], where flow next to the denticle surface is in the opposite direction to free stream flow due to the presence of a large separation bubble that forms on the foil. We should not assume that shark denticles or bony fish scales are designed to function with flow acting only in the free stream direction along their surface.

The extent to which individual scales are mobile during fish swimming is unknown, but fish lack direct muscular attachments to individual scales and so any scale mobility will be the result of external forces. Scale motion could certainly affect the boundary layer, and movement that does occur is most likely a passive response to body bending, to pressure changes within the body cavity, or to tension applied to dermal collagen fibers that invest the skin. Fish skin is remarkably complex and in this paper we have focused on the pattern of surface ornamentation in sharks and bony fishes. But fish skin also possesses an extensive dermal array of embedded collagen fibers [51,52], and some fish species have scales embedded within the dermis that will likely affect the material properties and hence the pattern of skin deformation during locomotion. The extent to which scale motion affects skin hydrodynamic function is unknown, but linking skin structure to locomotor hydrodynamics is a promising area for future work.

ACKNOWLEDGEMENTS

The authors would like to thank members of the Lauder Lab for assistance with this research, and Abby Noll, Spencer Garborg, and Erik Anderson (Grove City College) for discussions and experiments on fish surface flows and boundary layers. Many thanks to Johannes Oeffner for his collaborative original research on shark skin function. Katia Bertoldi, James C. Weaver, and August Domel acknowledge support from the National Science Foundation (DMR- 1533985). Thanks to Ren Ziyu (Beihang University) and Li Wuxia (Institute of Physics, Chinese Academy of Science) for helping to fabricate the Nanoscribe 3D printed shark skin denticle. Research on fishes was approved under Harvard IACUC 20-03. This work was supported by NSF grant EFRI-0938043 and ONR MURI Grant N000141410533 monitored by Dr. Bob Brizzolara to GVL, as well as NSF GRF 2014162421 awarded to DKW, and by Chinese National Science Foundation grant 61403012 to LW.

---

[1] K. F. Liem, W. E. Bemis, W. F. Walker, and L. Grande, *Functional Anatomy of the Vertebrates. An evolutionary perspective. Third Edition* (Harcourt College Publishers, Fort Worth, 2001).

[2] P. G. Allison *et al.*, Mechanical properties and structure of the biological multilayered material system, *Atractosteus spatula* scales, Acta Biomaterialia **9**, 5289 (2013).

[3] A. Bigi, M. Burghammer, R. Falconi, M. H. J. Koch, S. Panzavolta, and C. Riekel, Twisted plywood pattern of collagen fibrils in teleost scales: an X-ray diffraction investigation, Journal of structural biology **136**, 137 (2001).

[4] B. J. F. Bruet, J. Song, M. C. Boyce, and C. Ortiz, Materials design principles of ancient fish armour, Nature Mater. **7**, 748 (2008).

[5] B. Dean and B. Bhushan, Shark-skin surfaces for fluid-drag reduction in turbulent flow: a review, Philosophical Transactions of the Royal Society A: Mathematical, Physical and Engineering Sciences **368**, 4775 (2010).

[6] D. W. Bechert, M. Bartenwerfer, G. Hoppe, and W. E. Reif, Drag reduction mechanisms derived from shark skin, AIAA **2**, 1044 (1986).

[7] D. W. Bechert and W. Hage, in *Flow Phenomena in Nature. Volume 2. Inspiration, learning, and application*, edited by R. Liebe (WIT Press, Southampton, UK, 2007), pp. 457.

[8] C. C. Büttner and U. Schulz, Shark skin inspired riblet structures as aerodynamically optimized high temperature coatings for blades of aeroengines, Smart Mater. Struct. **20**, 094016 (2011).

[9] Y. Luo, X. Li, D. Zhang, and Y. Liu, Drag reducing surface fabrication with deformed sharkskin morphology, Surface Engineering (2015).

[10] A. Lang, P. Motta, M. L. Habegger, R. Hueter, and F. Afroz, Shark skin separation control mechanisms, Marine Tech. Soc. J. **45**, 208 (2011).

[11] L. Sirovich and S. Karlsson, Turbulent drag reduction by passive mechanisms, Nature **388**, 753 (1997).

[12] P. Luchini, F. Manzo, and A. Pozzi, Resistance of a grooved surface to parallel flow and cross-flow, J. Fluid Mech. **228**, 87 (2006).

[13] D. W. Bechert, M. Bruse, and W. Hage, Experiments with three-dimensional riblets as an idealized model of shark skin, Exp. Fluids **28**, 403 (2000).

[14] A. Boomsma and F. Sotiropoulos, Direct numerical simulation of sharkskin denticles in turbulent channel flow, Phys. Fluids **28**, 035106 (2016).

[15] G. Díez, M. Soto, and J. M. Blanco, Biological characterization of the skin of shortfin mako shark *Isurus oxyrinchus* and preliminary study of the hydrodynamic behaviour through computational fluid dynamics, J. Fish. Biol. **87**, 123 (2015).

[16] J. Videler, Body surface adaptations to boundary-layer dynamics, Symposia of the Society for Experimental Biology **49**, 1 (1994).

[17] D. W. Bechert, M. Bruse, W. Hage, J. G. T. Van Der Hoeven, and G. Hoppe, Experiments on drag-reducing surfaces and their optimization with an adjustable geometry, J. Fluid Mech. **338**, 59 (1997).

[18] E. J. Anderson, P. S. MacGillivray, and M. E. Demont, Scallop shells exhibit optimization of riblet dimensions for drag reduction, Biol. Bull. **192**, 341 (1997).

[19] L. Wen, J. C. Weaver, and G. V. Lauder, Biomimetic shark skin: design, fabrication, and hydrodynamic function, J. Exp. Biol. **217**, 1656 (2014).

[20] R. E. Shadwick and G. V. Lauder, *Fish Biomechanics* (Academic Press, San Diego, 2006), Vol. 23.

[21] R. Shadwick and S. Gemballa, in *Fish Biomechanics. Volume 23 in Fish Physiology*, edited by R. E. Shadwick, and G. V. Lauder (Academic Press, San Diego, 2006), pp. 241.

[22] G. V. Lauder, Fish locomotion: recent advances and new directions, Ann. Rev. Marine Sci. **7**, 521 (2015).

[23] P. Motta, M. L. Habegger, A. Lang, R. Hueter, and J. Davis, Scale morphology and flexibility in the shortfin mako *Isurus oxyrinchus* and the blacktip shark *Carcharhinus limbatus*, J. Morphol. **273**, 1096 (2012).

[24] W.-E. Reif, Squamation and Ecology of Sharks, Cour. Forsch.-Inst. Senckenberg **78**, 1 (1985).

[25] D. K. Wainwright and G. V. Lauder, Three-dimensional analysis of scale morphology in bluegill sunfish, *Lepomis macrochirus*, Zoology **119**, 182 (2016).

[26] L. Wen, J. C. Weaver, P. J. M. Thornycroft, and G. V. Lauder, Hydrodynamic function of biomimetic shark skin: effect of denticle pattern and spacing, Bioinsp. Biomimet. **10**, 1 (2015).

[27] R. Li and E. Adelson, in *Proceedings of the IEEE Conference on Computer Vision and Pattern Recognition*2013), pp. 1241.

[28] R. Li, R. Platt, W. Yuan, A. ten Pas, N. Roscup, M. A. Srinivasan, and E. Adelson, in *Intelligent Robots and Systems (IROS 2014), 2014 IEEE/RSJ International Conference on* (IEEE, 2014), pp. 3988.

[29] J. Oeffner and G. V. Lauder, The hydrodynamic function of shark skin and two biomimetic applications, J. Exp. Biol. **215**, 785 (2012).

[30] G. V. Lauder, E. J. Anderson, J. Tangorra, and P. G. A. Madden, Fish biorobotics: kinematics and hydrodynamics of self-propulsion, J. Exp. Biol. **210**, 2767 (2007).

[31] D. B. Quinn, G. V. Lauder, and A. J. Smits, Maximizing the efficiency of a flexible propulsor using experimental optimization, J. Fluid Mech. **767**, 430 (2015).

[32] G. V. Lauder, B. E. Flammang, and S. Alben, Passive robotic models of propulsion by the bodies and caudal fins of fish, Int. Comp. Biol. **52**, 576 (2012).

[33] R. M. Shelton, P. J. M. Thornycroft, and G. V. Lauder, Undulatory locomotion by flexible foils as biomimetic models for understanding fish propulsion, J. Exp. Biol. **217**, 2110 (2014).

[34] J. Lim and G. Lauder, Mechanisms of anguilliform locomotion in fishes studied using simple three-dimensional physical models, Bioinsp. Biomimet. **11**, 046006 (2016).

[35] S. Alben, C. Witt, T. V. Baker, E. J. Anderson, and G. V. Lauder, Dynamics of freely swimming flexible foils, Phys. Fluids **24**, 051901 (2012).

[36] L. Wen and G. V. Lauder, Understanding undulatory locomotion in fishes using an inertia-compensated flapping foil robotic device, Bioinsp. Biomimet. **8**, 046013 (2013).

[37] D. B. Quinn, G. V. Lauder, and A. J. Smits, Scaling the propulsive performance of heaving flexible panels, J. Fluid Mech. **738**, 250 (2014).

[38] D. B. Quinn, G. V. Lauder, and A. J. Smits, Flexible propulsors in ground effect, Bioinsp. Biomimet. **9**, 1 (2014).

[39] J. I. Castro, *The Sharks of North America* (Oxford Univ. Press, Oxford, 2011).

[40] K. N. Lucas, P. Thornycroft, B. J. Gemmell, S. P. Colin, J. H. Costello, and G. V. Lauder, Effects of non-uniform stiffness on the swimming performance of a passively-flexing, fish-like foil model, Bioinsp. Biomimet. **10**, 056019 (2015).

[41] I. Borazjani and M. Daghooghi, The fish tail motion forms an attached leading edge vortex, Proceedings. Biological sciences / The Royal Society **280**, 20122071 (2013).

[42] C. D. Wilga and G. V. Lauder, Three-dimensional kinematics and wake structure of the pectoral fins during locomotion in leopard sharks *Triakis semifasciata*, J. Exp. Biol. **203**, 2261 (2000).

[43] C. D. Wilga and G. V. Lauder, Functional morphology of the pectoral fins in bamboo sharks, *Chiloscyllium plagiosum*: benthic versus pelagic station holding, J. Morphol. **249**, 195 (2001).

[44] A. W. Lang, M. T. Bradshaw, J. A. Smith, J. N. Wheelus, P. J. Motta, M. L. Habegger, and R. E. Hueter, Movable shark scales act as a passive dynamic micro-roughness to control flow separation, Bioinsp. Biomimet. **9**, 036017 (2014).

[45] A. W. Lang, P. Motta, P. Hidalgo, and M. Westcott, Bristled shark skin: a microgeometry for boundary layer control?, Bioinsp. Biomimet. **3**, 046005 (2008).

[46] B. J. Gemmell, S. P. Colin, J. H. Costello, and J. O. Dabiri, Suction-based propulsion as a basis for efficient animal swimming, Nature Commun. **6** (2015).

[47] E. J. Anderson, W. McGillis, and M. A. Grosenbaugh, The boundary layer of swimming fish, J. Exp. Biol. **204**, 81 (2001).

[48] U. Ehrenstein and C. Eloy, Skin friction on a moving wall and its implications for swimming animals, J. Fluid Mech. **718**, 321 (2013).

[49] U. Ehrenstein, M. Marquillie, and C. Eloy, Skin friction on a flapping plate in uniform flow, Philosophical Transactions of the Royal Society of London A: Mathematical, Physical and Engineering Sciences **372**, 20130345 (2014).

[50] K. Yanase and P. Saarenrinne, Unsteady turbulent boundary layers in swimming rainbow trout, J. Exp. Biol. **218**, 1373 (2015).

[51] P. J. Motta, Anatomy and functional morphology of dermal collagen fibres in sharks, Copeia **1977**, 454 (1977).

[52] S. A. Wainwright, F. Vosburgh, and J. H. Hebrank, Shark skin: function in locomotion, Science **202**, 747 (1978).

FIGURES and CAPTIONS

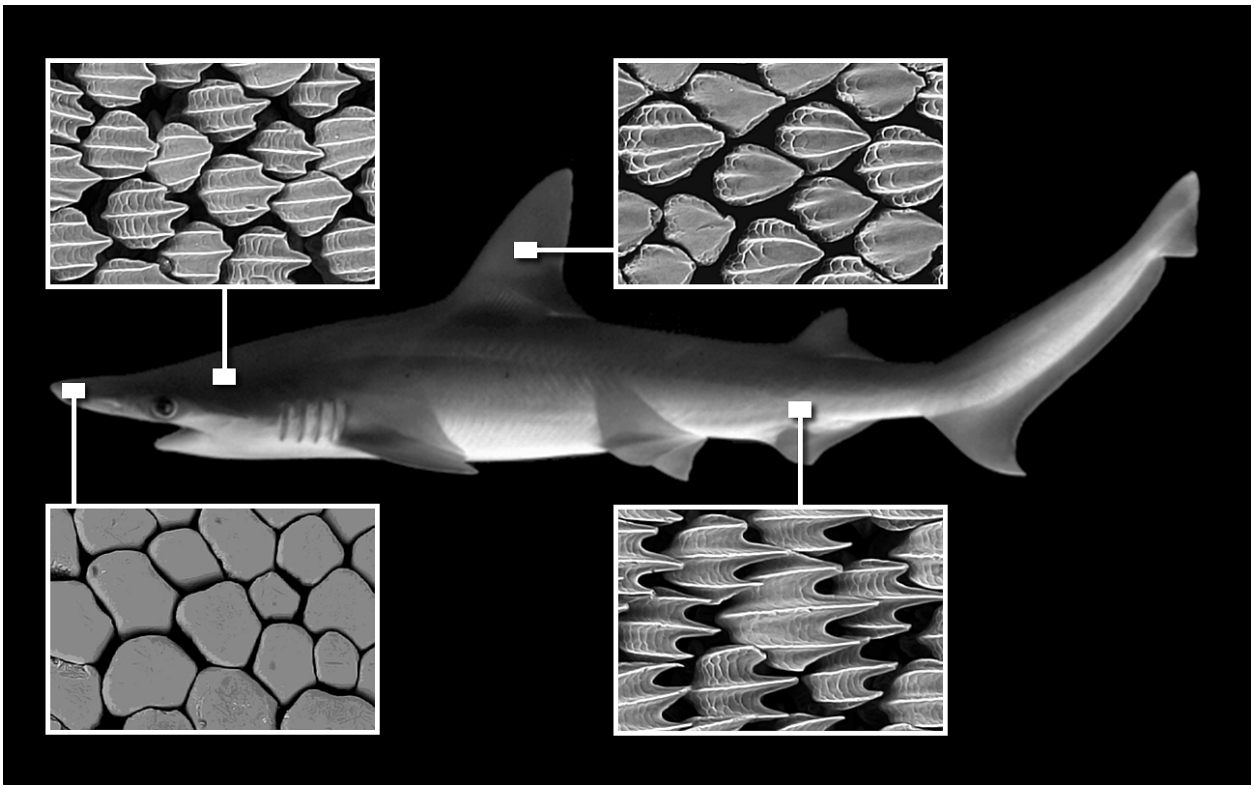

FIG. 1. Scanning electron micrographs (SEM) showing the diversity of denticles around the body and head of a bonnethead shark, *Sphyrna tiburo*. Individual denticles are all 100 - 200 μm in length [see 19,29]. Denticles near the leading edge of the head are flatter with greatly reduced or absent ridges, while denticles on the mid- and posterior-body regions have prominent ridges and posterior projections oriented in the stream-wise direction.

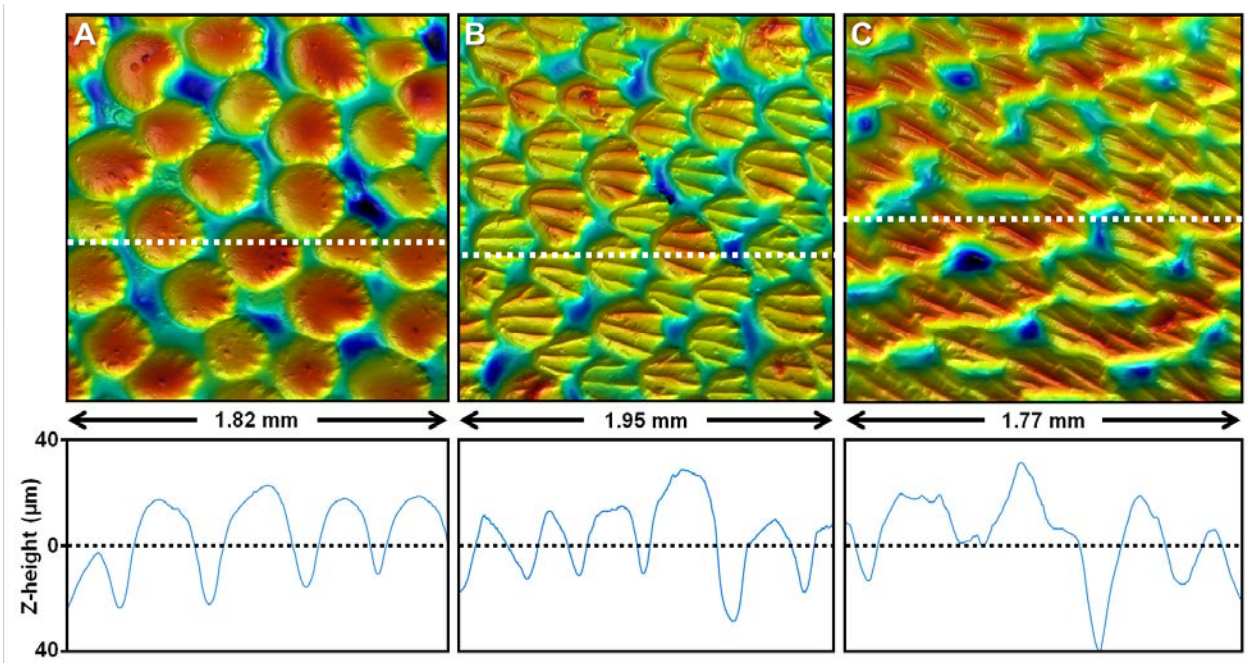

FIG. 2. Surface topography of a blue shark (*Prionace glauca*). A, surface of the dorsal side of the anterior-most tip of the head. B, topography of the dorsal side of the head between the eyes. C, topography of denticles from the trailing edge of the tail. All images are arranged so that anterior is left, and dorsal is up; color indicates surface height, with blue representing the lowest regions, and red color the regions that project the greatest extent from the surface. Dotted lines in each image show the location of the vertical profiles below each image. Shark surface roughness varies considerably around the body.

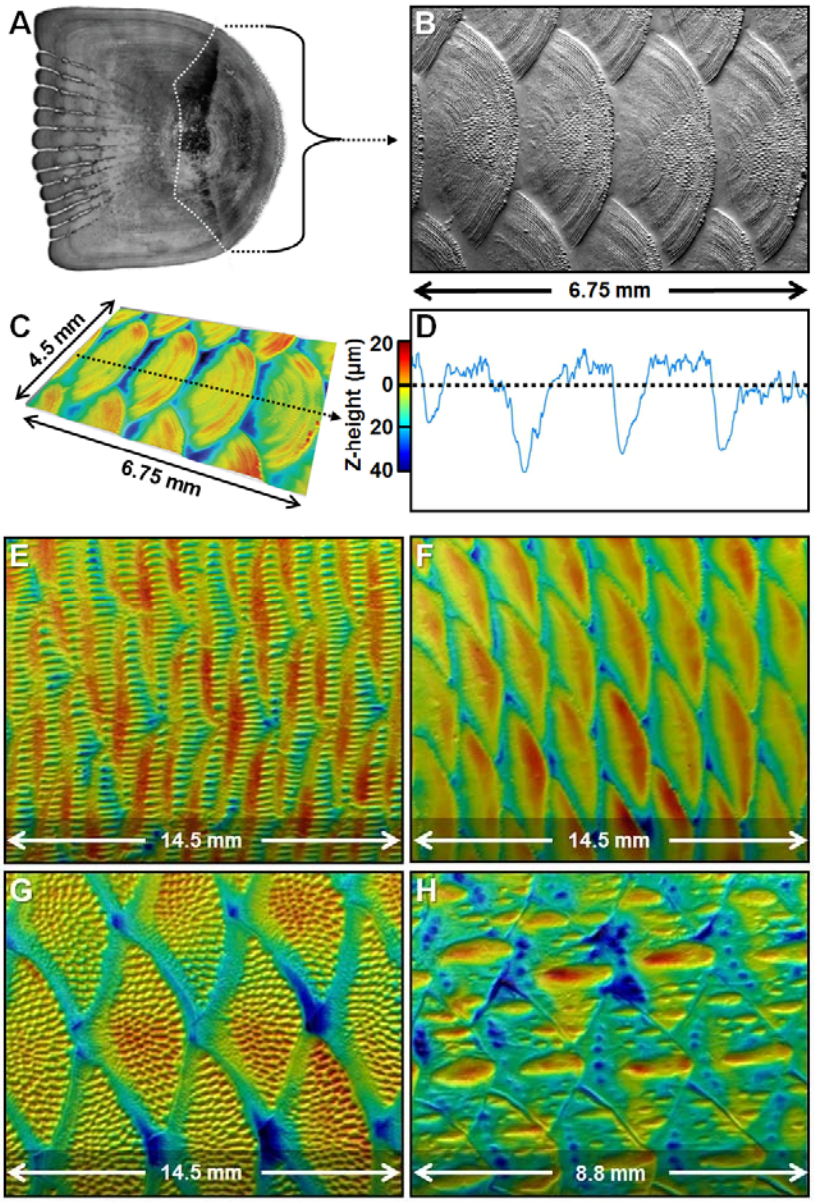

FIG. 3. Bony fish surfaces. A, photograph of a single bluegill sunfish (*Lepomis macrochirus*) scale (dashed white line indicates the limit of the portion of the scale exposed to the water). B, group of scales located in the center of the body from a bluegill sunfish to show the overlapping arrangement. C, a 45 degree view with height enhanced (by 3%) of the same image in A, with a vertical profile along the dashed line shown to the right. E, the surface of a gulf menhaden (*Brevoortia patronus*). F, the surface of a Hawaiian dascyllus (*Dascyllus albisella*). G, the surface of a sargassum triggerfish (*Xanthichthys ringens*) just posterior to the tip of the pectoral fin. H, the surface of a rainbow smelt (*Osmerus mordax*). All images show surfaces where anterior is left and dorsal is up. For images C, E – H, color indicates height with dark blue representing the lowest point, and red the highest point on the fish surface. Maximum feature height ranges from ~150 µm to 350 µm.

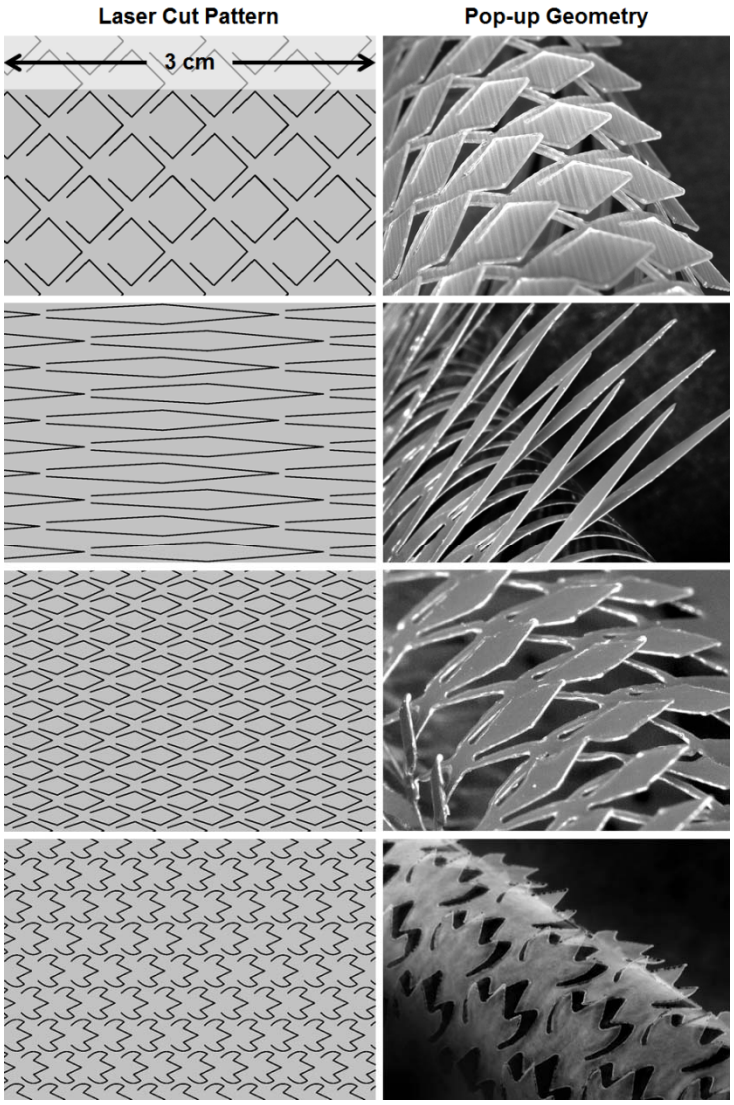

FIG. 4. Two-dimensional biomimetic foils with different patterns laser-cut into thin flexible plastic panels. Images in the left column show the cut pattern (all illustrated at the same scale), used to generate deformable fish scale-like components. Images to the right show bent foils and the resulting pop-up geometry. Water can flow from one side to the other of the swimming foil when the cut elements deform. Patterns are cut into different thickness plastic materials to vary the extent of the pop-up behavior during bending. From top to bottom, foil thicknesses are 0.19 mm, 0.05 mm, 0.05 mm, and 0.025 mm.

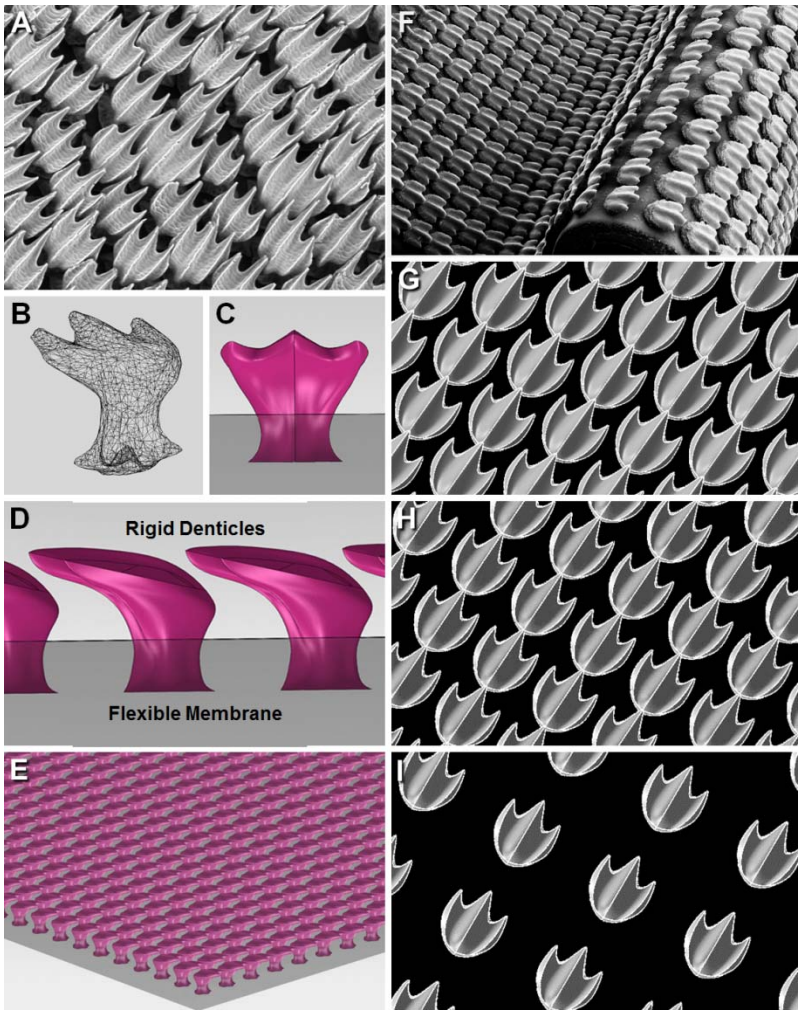

FIG. 5. Shark denticle models and biomimetic skin membranes. A, Bonnethead shark (*Sphyrna tiburo*) denticles from near the anal fin (scales are ~ 200 μm in length). B, three-dimensional mesh and rendered model (C) of an individual denticle. D, a row of denticles, showing how the top of one denticle overlaps the base of the adjacent one. E, two-dimensional denticle array in which rigid denticles are laid out on a flexible membrane substrate. F, fabricated biomimetic synthetic shark skin membrane used for hydrodynamic testing in which rigid denticles are arrayed on a flexible substrate. Individual denticles are ~1 mm in length. G, H, I, diagrams of three different denticle patterns and densities used for testing the effect of changing denticle arrangements on propulsion. Adapted from [19,22,26,29].

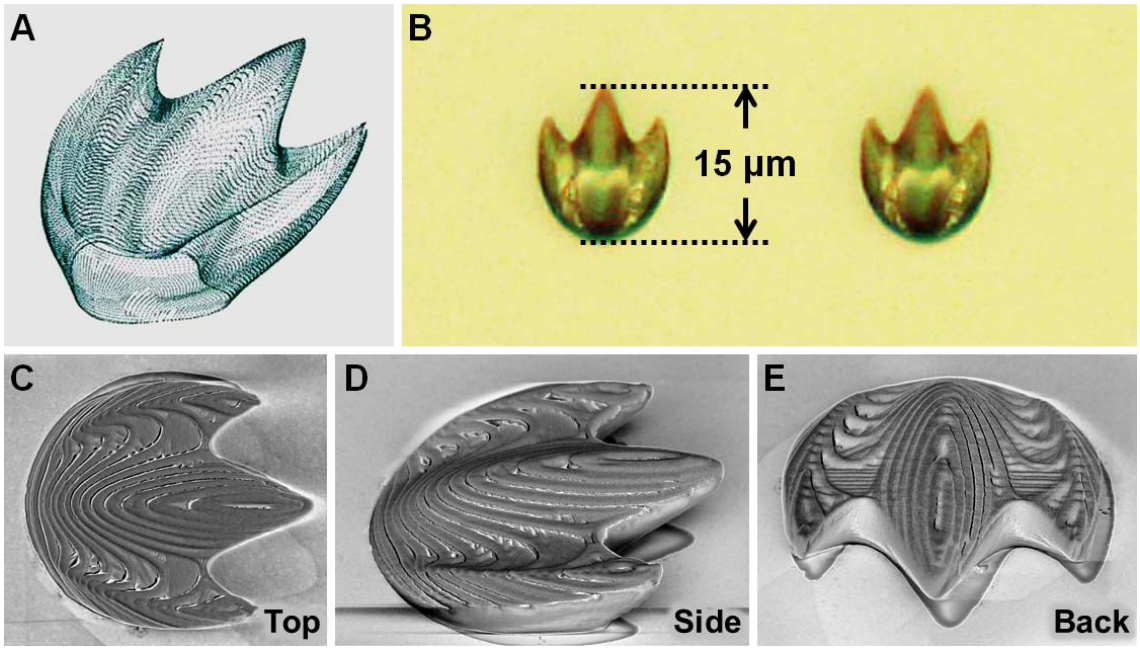

FIG. 6. Images of a high-resolution 3D print of a shark skin denticle. (A) Volumetric model of a denticle generally similar to those of mako sharks (*Isurus oxyrinchus*). (B) Optical microscopic image of the fabricated denticle in top view showing the size scale. Scanning electron microscopic images of the denticle are shown in top (C), side (D), and posterior (E) views. The 3D printed denticle is mounted on a glass coverslip, and manufactured using two-photon lithography.

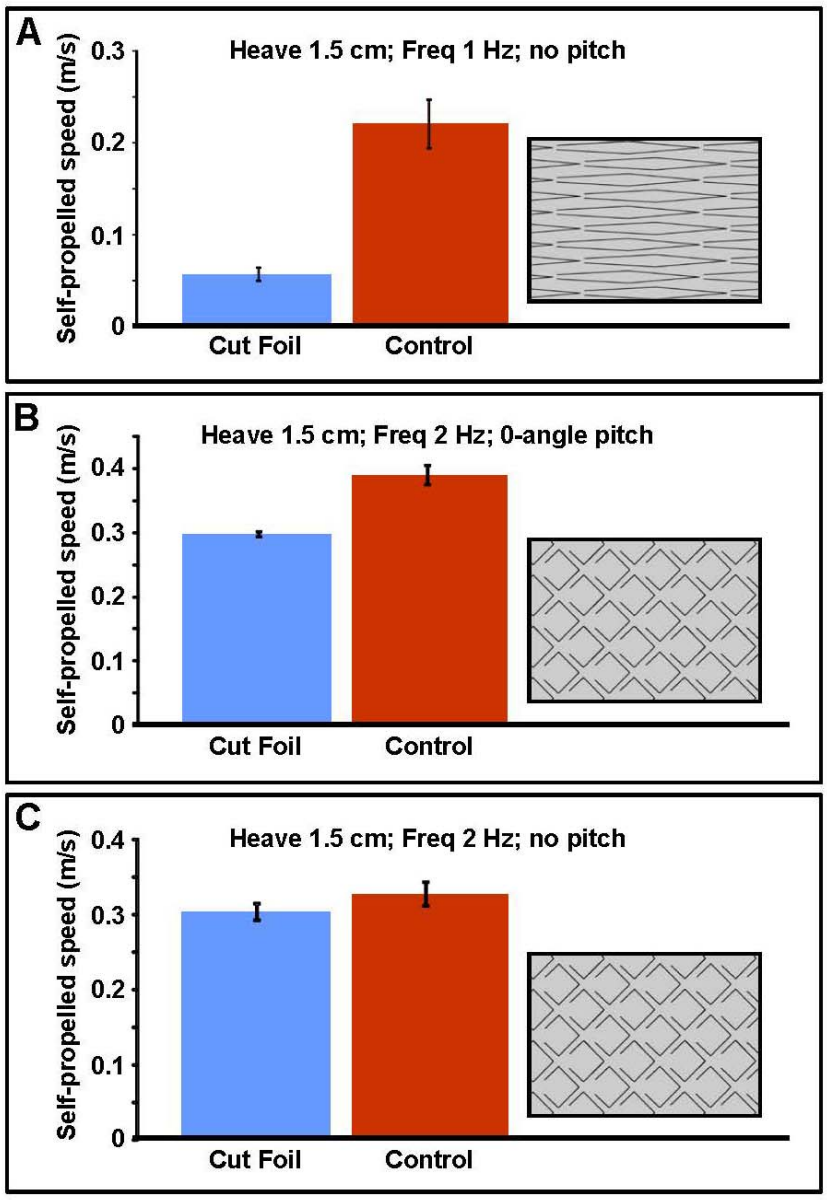

FIG. 7. Analysis of self-propelled swimming speeds for two of the two-dimensional cut foils shown in Fig. 4. The three motion programs used for testing are explained in the text. Images to the right show the foil cut pattern for each test condition. Error bars are +/- one standard error. Cost of transport (J/m) for each foil type: A, control (0.021), cut foil (0.096); B, control (0.045), cut foil (0.047); C, control (0.104), cut foil (0.108).

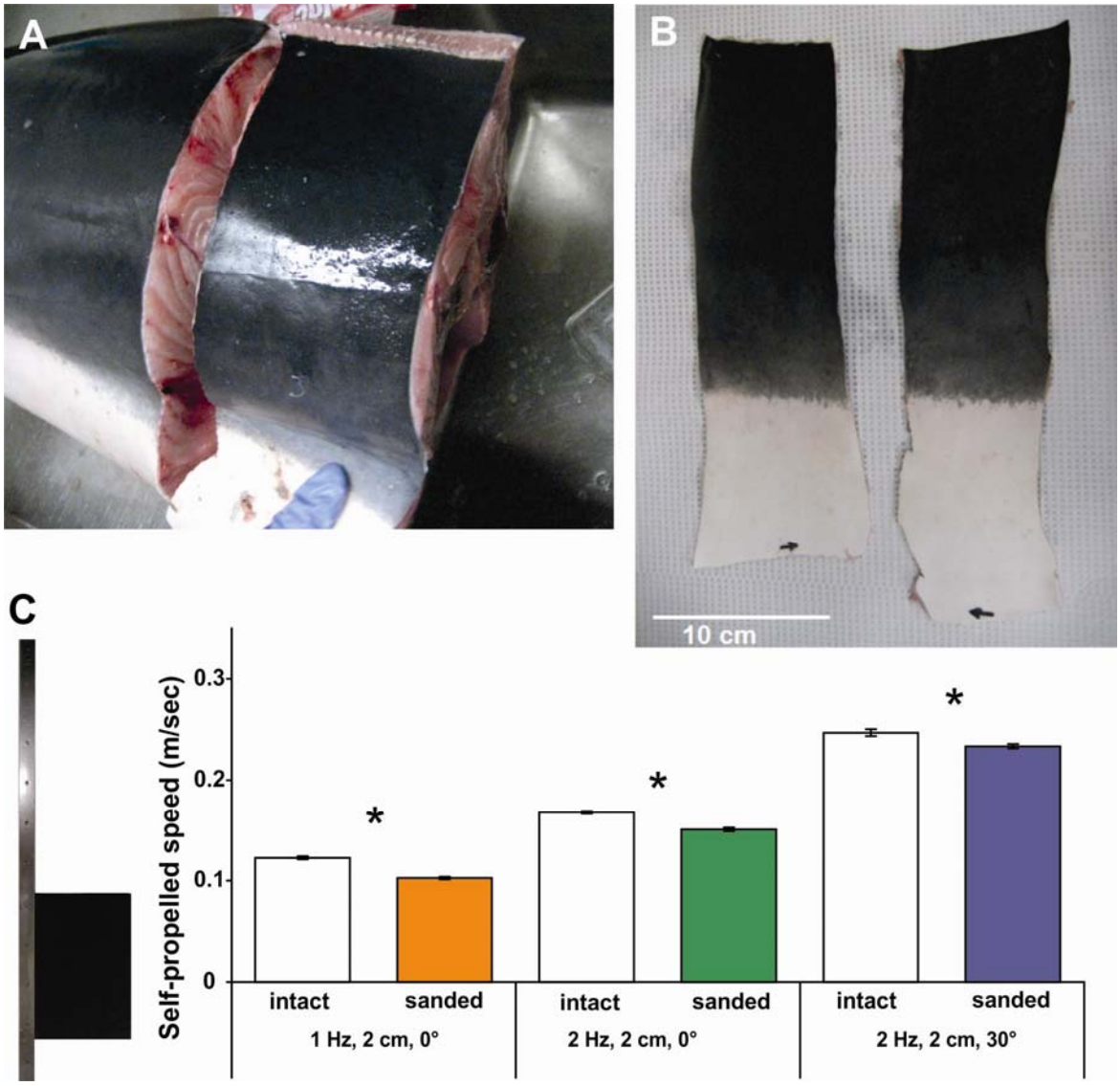

FIG 8. Fabrication of a flexible skin foil from mako shark skin, and analysis of the self-propelled swimming speed of this foil under three motion programs, compared to a smoother sanded foil in which most of the denticles have been removed. A, removal of sections of skin from a mako shark (*Isurus oxyrinchus*). Skin is then cleaned of underlying tissue (B) and the orientation marked (black arrow at the bottom of each skin strip). Two skin strips are glued to each other with each denticle surface facing the water, trimmed into a rectangular flexible foil, and attached to a rod for testing (C). Histograms show the self-propelled swimming speed for three different motion programs in which the leading edge of the shark skin foil is moved in heave (either 1Hz or 2Hz at +/- 2 cm), and with no pitch or with 30° pitch. In each of the three tested cases, the intact shark skin foil swims significantly faster than the smoother control (*). Adapted in part from [29]; photographs in (A) and (B) courtesy of Johannes Oeffner.

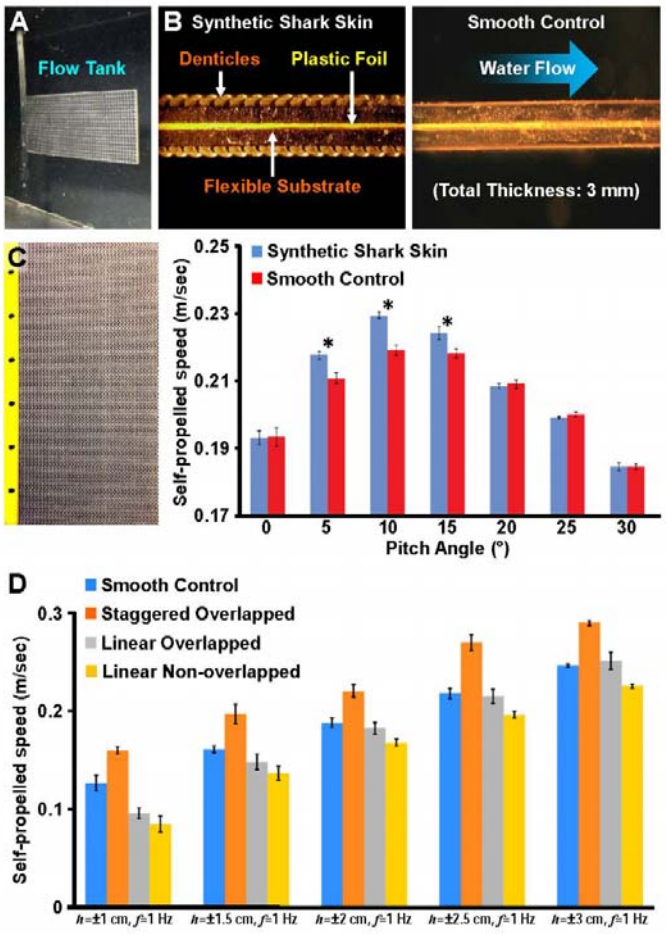

FIG. 9. Hydrodynamic function of biomimetic shark skin models. A, Dynamic testing in a flow tank of a synthetic shark skin membrane in a mechanical flapping controller. B, cross-sections of biomimetic shark skin and the smooth control, both manufactured to be of equal total mass; blue arrow indicates the direction of water flow. C, a flexible plastic foil (yellow, 0.5 mm thickness) is covered on both sides with 3D printed flexible synthetic shark skin to allow testing; foil is 177 mm in height and 77 mm chord width. Histogram shows results of testing the self-propelled speed of this synthetic shark skin membrane with respect to the smooth control surface at different leading edge pitch values; heave amplitude was ± 1.5 cm and frequency was 1 Hz for all tests. At pitch angles of 5°, 10°, and 15° (asterisks), the swimming speeds of the biomimetic shark skin foils were significantly greater than those of the controls; at the other four pitch angles, the swimming speeds were similar. D, tests of the swimming speeds of three different denticle patterns (see Fig. 5) relative to a smooth control at five different leading edge heave values. Error bars represent ±1 standard error of the mean. Adapted in part from [19,26].

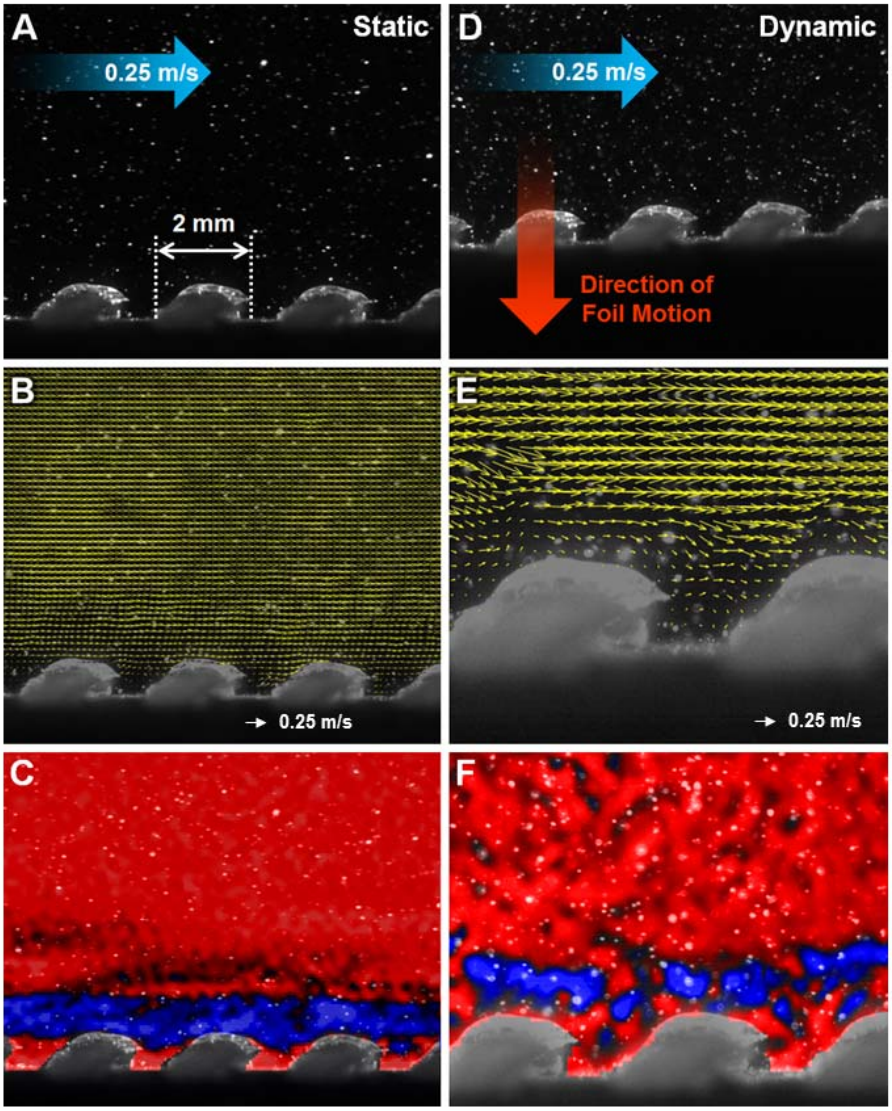

FIG. 10. Flow over a synthetic shark skin membrane with widely spaced denticles (see Figure 5I) during static testing (A-C) and under dynamic conditions of 2 Hz leading edge oscillation and a free stream flow of 25 cm/s (D-F). Top images show the biomimetic shark skin membrane; blue and red arrows indicate the direction of water and foil motion respectively. Middle panels show velocity vector fields representing flow over the membrane. C, average vorticity (mean over 0.4 s) on the surface of the static shark skin panel; vorticity (s^{-1}) ranges from maximum positive (red) of 0.025 to maximum negative (blue) of -0.4. F, instantaneous vorticity (s^{-1}) over the shark skin panel surface; vorticity ranges from maximum positive (red) of 120 to maximum negative (blue) of -400. Size of the denticles is shown in panel A.